Construction of high performance CH3NH3PbI3-based solar cells by hot-casting technique

Wang, Shiwei; Wang, Lijuan; Zhang, Long; Chang, Lei; Wang, Le; Wang, Junling

2017

Wang, S., Wang, L., Zhang, L., Chang, L., Wang, L., & Wang, J. (2017). Construction of high performance CH3NH3PbI3-based solar cells by hot-casting technique. Solar Energy Materials and Solar Cells, 163, 120-124.

https://hdl.handle.net/10356/83487

https://doi.org/10.1016/j.solmat.2017.01.009

Construction of high performance $CH_3NH_3PbI_3$-based solar cells by hot-casting technique

Shiwei Wang[a,*], Lijuan Wang[a], Long Zhang[a], Lei Chang[b], Le Wang[b], Junling Wang[b,*]

a School of Chemical Engineering, Advanced Institute of Materials Science, Changchun University of Technology, Changchun 130012, PR China

b School of Materials Science and Engineering, Nanyang Technological University, 639798, Singapore

Abstract

Two-dimensional plane $CH_3NH_3PbI_3$ crystals in millimeter size have been first successfully constructed on FTO glass coated with mesoporous TiO_2 by hot-casting technique. Depending on the closely and continuous arrangement of large perovskite crystals in the film, a best power conversion efficiency (PCE) of 16.01% was achieved along with a photocurrent density of 21.32 mA/cm2, an open circuit voltage of 1.07 V and a fill factor of 0.70 from the corresponding CH3NH3PbI3-based solar cells with p-i-n structure. Even more exciting was the quite good stability of the hot-casting-based device, which remained at more than 91% under 55% humidity for 10 days.

Key words: $CH_3NH_3PbI_3$; Perovskite solar cells; Hot-casting technique; Crystal

1. Introduction

Organic-inorganic hybrid perovskite solar cells have attracted considerable attention in recent years because of the numerous desirable properties, which are promising candidate for next generation photovoltaic technology [1-4]. From the beginning of 2014, the power conversion efficiency (PCE) of perovskite solar cells based on $CH_3NH_3PbI_3$ structure up to higher than 20% has been achieved on both planar and mesoporous structures [5, 6]. In order to improve the performance of the device, several technologies have been developed for the preparation of high quality

perovskite thin films, such as: one-step spin-coating, two-step sequential solution deposition, vapor-assisted solution process, dual-source vapor deposition in a high-vacuum chamber and so on [7-10]. However, the size of perovskite crystal was usually between tens of nanometers to several microns, so it was easy to form pinholes on the film. This not only caused electrical shorting but also deleteriously impacted charge dissociation/transport/recombination for devices [11-14]. In addition, based on the stability and reliability of the device, planar-hetero-junction perovskite solar cells with mesoporous architecture have been widely recognized in practical research and application [15, 16]. Thus, a series of basic problems regarding the device structure and material properties in perovskite-based device have been attracting more and more researchers' interests. Among them, it can be concluded that large crystal size, full coverage and compact aggregation morphology of perovskite films were rather important for high performance perovskite solar cells [17-20].

In this work, two-dimensional $CH_3NH_3PbI_3$ crystals in millimetre size have been successfully constructed on mesoporous TiO_2 (m-TiO_2) surface by hot-casting methods. By controlling the process conditions, $CH_3NH_3PbI_3$ crystals were continuous and aggregated closely in the film. A best power conversion efficiency (PCE) of 16.01% was achieved along with a photocurrent density of 21.32 mA/cm^2, a voltage of 1.07 V and a fill factor of 0.70 from the corresponding $CH_3NH_3PbI_3$-based solar cells with FTO/block TiO_2/m-TiO_2/$CH_3NH_3PbI_3$/Spiro-OMeTAD structure. The hot-casting process was simple and efficiency. It needed only a few seconds and microliters of precursor solutions in the whole procedure. Excellent stability of the hot-casting-based device has also been detected, the PCE of which remained at more than 91% (from 16.01% to 14.59%) under 55% humidity ambient condition for 10 days, whereas the one prepared by two-step method was decayed from ~12.50 % to 1 % over 7 days. More important, the large two-dimensional plane $CH_3NH_3PbI_3$ crystals must be much more meaningful research work in theory and other optoelectronic devices.

2. Experimental

Methylammonium iodide (MAI) was synthesized according to the literature reported in previous [21]. CH_3NH_3I was synthesized in ice bath by adding hydroiodic acid (HI, 57 wt% in water, Sigma-Aldrich) into methylamine (33 wt% in ethanol, Sigma-Aldrich) and stirring for 2 h. The precipitate was washed by dissolving in a minimum amount of ethanol and then adding in a large amount of diethyl ether. The precipitate was collected by filtration. The procedure was repeated three times to get pure MAI. The resulting product (white powder) was dried at 60 °C. The perovskite precursor was prepared by mixing MAI and PbI_2 (99%, Sigma-Aldrich) in a molar ratio of 1:1 in anhydrous N. N-dimethylformamide (DMF; 99.99%, Sigma-Aldrich) or γ-butyrolactone (GBL; 99.99%, Sigma-Aldrich), and the final concentration of the perovskite was controlled to approximately 100 mg/mL. FTO substrates were cleaned sequentially with detergent, deionized water, acetone, ethanol, and isopropyl alcohol under ultrasonic for 10 min. TiO_2 compact layer was then deposited on the substrates by aerosol spray pyrolysis at 450 °C using a commercial titanium diisopropoxide bis (acetylacetonate) solution (75% in 2-propanol, Sigma-Aldrich) diluted in ethanol (1:39, volume ratio) as precursor and oxygen as carrier gas. The m-TiO_2 layer composed of 20-nm-sized particles was deposited by spin-coating at 5,000 rpm for 30 s using a commercial TiO_2 paste (Dyesol 18-NRT, Dyesol) diluted in ethanol (2:7, weight ratio). After drying at 125 °C, the TiO_2 films were gradually heated to 500 °C, baked at this temperature for 15 min.

As shown in Scheme 1, the FTO substrate was placed on the hot stage for more than ten minutes to ensure that the substrate was heated completely. Then move the substrate onto the prepared spin-coating apparatus suddenly. 80 μL of $CH_3NH_3PbI_3$ precusor solution (100 mg/mL) was dropped to the substrate under the condition of high speed rotating (4000 rpm for 5 s).

After moving the sample to another plate in room temperature in fast speed, the film sample turn reddish brown color in 3 mins because of the formation of large $CH_3NH_3PbI_3$ crystal.

3. Results and disscussion

The morphology of m-TiO_2 film and $CH_3NH_3PbI_3$ film was characterized by scanning electron microscope (SEM) and polarizing microscope. As shown in Fig. 1A, the SEM image of m-TiO_2 films with 20 nm of holes was the same as literature reported. In another, the boiling point of the solution was very important for the formation of large $CH_3NH_3PbI_3$ crystals and high quality film in the process of hot-casting technique. When the $CH_3NH_3PbI_3$ precursor solution was dipped out and contacted with the rotating substrate surface in high temperature, the major solvent in the precursor solution would be volatilized. Large crystals would be formed immediately after the sample was moved onto a room temperature plate in fast speed. Note that $CH_3NH_3PbI_3$ crystals were not only grown toward plane direction and compact accumulation in the film but also could fully fill the hollows of m-TiO_2 layer. Accordingly, the specific film morphology in hot-casting technique was attributed to the sudden temperature changes. If the temperature was not high enough, too much solvent would be left on the film after hot spin coating, so the corresponding crystals formed on the film would be not fully and not good enough after left it in room temperature, the microscope photos of which can be seen in Fig. 1A and Fig. 1B. Oppositely, if the temperature was too high, all of the solvent would be volatilized and some crystals formed on the film would be destroyed (as shown in Fig. 1C). So, 175 °C was selected as the proper temperature to fabricate excellent $CH_3NH_3PbI_3$ film for DMF solvent by this technique. After careful observation, it can be seen that the scale of $CH_3NH_3PbI_3$ crystals in the film can reach as high as 0.5 mm. As contrast, the crystal scale of $CH_3NH_3PbI_3$ prepared on FTO/m-TiO_2 substrate by the popular two-step method was less than 500 nm (Fig. 1B). The process of preparing $CH_3NH_3PbI_3$ films by two-step method were described in Supporting Information (SI).

In order to confirm the applicability and regulation of the hot-casting technique further, another typical polar solvent of GBL was also used to repeat the process. Large $CH_3NH_3PbI_3$ crystals were also formed on the film in the same way which can be seen from Fig. 1G-J, but the crystal size was obviously smaller than the one from DMF solvent. That is because the boiling point of GBL is higher than DMF, and

$CH_3NH_3PbI_3$ have better solubility in GBL than in DMF, so the crystal is not easy to be separated out suddenly.

It can be concluded that the morphology of $CH_3NH_3PbI_3$ films can be controlled by the growth way of perovskite crystals, which determined the properties of the films. Fermi level of the flat film with full surface coverage on TiO_2 was closer to the middle of the band-gap, as compared to the rough perovskite film with partial coverage on TiO_2. As literatures reported, the $CH_3NH_3PbI_3$ film with large sized crystal and full surface coverage should have higher light harvesting in the visible spectral range, faster electron extraction rate, and lower defect density, resulting in better photoelectric response in the range of 500-800 nm and higher power conversion efficiency [22].

The samples of hot-casting $CH_3NH_3PbI_3$ film (DMF solution) deposited on FTO substrates coated with m-TiO_2 was further characterized by X-ray diffraction (XRD) and the diffraction patterns are shown in Fig. 2a. Obviously, strong diffraction peaks located at 14.1^o, 28.5^o and 31.8^o for 2 h scan are observed corresponding to the planes of (110), (220) and (310), which are rather consistent with previous reports [23, 24], so it can be indicated that the tetragonal perovskite structure has been formed. In another, XRD characterization of $CH_3NH_3PbI_3$ prepared using GBL solution was also provided to confirm the crystallization of $CH_3NH_3PbI_3$. As shown in Fig. S1, the diffraction peaks were completely consistent with the sample fabricated by DMF solution, which confirmed that no excess impurities in the perovskite film.

The thickness of $CH_3NH_3PbI_3$ films is important for their devices [25, 26], which can be controlled by the speed of spin-coating. Different speeds of spin-coating have been tried on hot substrate in our work, the results have been shown in Fig. 2b. It can be seen that the thickness of perovskite film is decreasing with the speed increasing of spin-coating. 80 μL of $CH_3NH_3PbI_3$ precursor solution (100 mg/mL in DMF) was used to drop on the substrates during the hot-casting process. The thickness of the $CH_3NH_3PbI_3$ film can reach 320 nm under the speed of 4000 rpm/s, and the best quality films with full coverage have been achieved in this condition. According to the literature report, 300 nm to 400 nm of active layer was an ideal thickness for high

performance perovskite solar cells [27-29]. The thickness of the $CH_3NH_3PbI_3$ layer was measured by section SEM technique, which is shown in Fig. S2.

Fig. 3a depicts the device structure of $CH_3NH_3PbI_3$-based solar cells, in which, $CH_3NH_3PbI_3$ was fabricated by hot-casting process on FTO glass substrates coated with block TiO_2 and m-TiO_2 layer. Subsequently, the Spiro-OMeTAD-based hole-transfer layer (80.0 mg spiro-OMeTAD, 28.5 ml 4-tert-butylpyridine and 17.5 ml lithium-bis (tri-fluoromethanesulfonyl) imide (Li-TFSI) solution (520.0 mg Li-TFSI in 1.0 ml acetonitrile) all dissolved in 1.0 ml chlorobenzene) was deposited by spin-coating at 4000 rpm for 30 s. Finally, a 100-nm-thick gold layer was deposited by thermal evaporation [30].

The average performance were measured from a batch of 40 devices, corresponded to a short-circuit photocurrent density (*Jsc*) of 21.32 mA/cm^2, an open-circuit voltage (*Voc*) of 1.07 V, and a fill factor (*FF*) of 0.70, leading to an PCE of 16.01% (with a standard deviation of only 0.92%) under AM 1.5 solar illumination at 100 mW/cm^2. The corresponding I-V curves are presented in Fig. 3b. The responsibility of devices can be guaranteed from the histogram of efficiencies as shown in Fig 3c. As contrast, the performances of the corresponding $CH_3NH_3PbI_3$-based solar cells prepared by two-step technique as usual described have also been tested in our lab, which was as shown in Table 1 (The efficiency was only 12.50% was achieved). The *Jsc* of the hot-casting-based device was obviously higher than the two-step-based device, because the conductivity for $CH_3NH_3PbI_3$ film with large perovskite crystal was better than the small one. And photovoltaic parameters of devices based on GBL solvent are obviously less than the ones based on DMF solvent, because the crystal size and aggregation morphology for the films fabricated by DMF were better than by GBL. The results also confirmed that the device efficiency increased with the increase of the crystal size of the films. The conclusion has been further characterized by optical absorption spectrum, which can be seen from Fig. S3. It can be noted that current density-voltage (J-V) curves were measured in air using a Keithley 2400 sourcemeter under the standard 1 sun AM 1.5 G simulated solar irradiation (100 mW/cm^2 from an Newport 91160A 300 W Solar Simulator (Class A). The simulated

solar irradiance is corrected by a Schott visible-color glass-filtered (KG5 colour filter) Si diode (Hamamatsu S1133). These encouraging results again demonstrate that large-size crystals, continuous and close aggregates morphology of perovskite film are propitious to PCE improvement for their devices. A typical EQE curve was shown in Fig S4. The EQE spectrum integration over the AM 1.5 G solar spectrum (100 mW/cm^2) yields a Jsc of ~22 mA/cm^2 (Fig. S4), which is consistent with the Jsc obtained from the J-V sweep.

Device stability has been also tested in ambient conditions at 55% relative humidity with complete devices without encapsulation. Current-voltage curves were recorded at 10 % illumination intensity to avoid any unwanted heating of the device during measurements. As shown in Fig. 3d, the PCE of the pristine perovskite device prepared by two-step method is seen to decay from ~12 % to 1 % over the first week, whereas that of the hot-casting-based device remains at more than 91% (from 16.01% to 14.59%) after 10 days later. Moisture was effectively prevented from penetrating further into the perovskite film due to the dense crystal structure, which greatly enhanced its chemical stability. In another, two dimensional $CH_3NH_3PbI_3$ crystals was regular, closely packed together in the film, so performances of the device fabricated in the film was repeatable no matter what position is deposited on the electrode. It can be sure that the excellent stability of the hot-casting-based device was also attributed to the dense crystal structure of the perovskite film.

4. Conclusions

Two dimensional plane $CH_3NH_3PbI_3$ crystals in large scale and dense accumulation of the film have been successfully constructed on m-TiO_2 surface by hot-casting methods. The PCE of the corresponding photovoltaic solar cells based on FTO/Block-TiO_2/m-TiO_2/$CH_3NH_3PbI_3$/Spiro-OMeTAD/Au structure can reach 16.01%. Excellent stability of the hot-casting-based device has also been detected, the PCE of which remained at more than 91% under 55% humidity ambient condition for 10 days. The process of the hot-casting technique was rather simple and efficiency,

because only several seconds are needed for the whole film fabrication procedure. In another, the large two-dimensional plane $CH_3NH_3PbI_3$ crystals will have much more meaningful research work in theory and other optoelectronic devices.

5. Acknowledgements

The authors gratefully acknowledge the funding of this research by the National Natural Science Foundation of China (Grant nos. 21204087, 21403016). Project Funded by China Postdoctoral Science Foundation (2015M570022). Scientific Research Foundation of Education Department of Jilin Province of China (2016326). Ministry of Education, Singapore under project No. MOE2013-T2-1-052 and AcRF Tier 1 RG126/14.

6. References

[1] N.G. Park, Materials Today, 18 (2015) 65-72.

[2] Q.F. Dong, Y.J. Fang, Y.C. Shao, P. Mulligan, J. Qiu, L. Cao, J.S. Huang, Science, 347 (2015) 967-970.

[3] S.Q. Luo and W.A. Daoud, J. Mater. Chem. A, 3 (2015) 8992-9010.

[4] Z.W. Gu, L.J. Zuo, T.T. Larsen-Olsen, T. Ye, G. Wu, F.C. Krebs, H.Z. Chen, J. Mater. Chem. A, 3 (2015) 1-8.

[5] W.S. Yang, J.H. Noh, N.J. Jeon, Y.C. Kim, S.C. Ryu, J.W. Seo, S.I. Seok, Science, 348 (2015) 1234-1237.

[6] M. Saliba, T. Matsui, J.Y. Seo, K. Domanski, J.P. Correa-Baena, M.K. Nazeeruddin, S.M. Zakeeruddin, W. Tress, A. Abate, A. Hagfeldt, M. Grätzel, Energy & Environmental Science, 9 (2016) 1989-1997.

[7] W. Chen, Y.Z. Wu, Y.F. Yue, J. Liu, W.J. Zhang, X.D. Yang, H. Chen, E.B. Bi, I. Ashraful, M. Grätzel, L.Y. Han, Science, 350 (2015) 944-948.

[8] H. S. Jung and N. G. Park, Small, 11 (2015) 10-25.

[9] T. Salim, S.Y. Sun, Y.C. Abe, A. Krishna, A.C. Grimsdale and Y.M. Lam, J. Mater. Chem. A, 3 (2015) 8943-8969.

[10] B. Yang, O. Dyck, J. Poplawsky, J. Keum, A. Puretzky, S. Das, I. Ivanov, C. Rouleau, G. Duscher, D. Geohegan, K. Xiao, J Am Chem Soc. 137 (2015) 9210-9213.

[11] Y.Y. Zhou, M.J. Yang, W.W. Wu, A.L. Vasiliev, K. Zhu, N. P. Padture, J. Mater. Chem. A, 3 (2015) 8178-8184.

[12] C. Bi, Q. Wang, Y.C. Shao, Y.B. Yuan, Z.G. Xiao, J.S. Huang, Nature Communications, 6 (2015) 7747.

[13] W.Y. Nie, H. Tsai, R. Asadpour, J.C. Blancon, A.J. Neukirch, G.Gupta, J.J. Crochet, M. Chhowalla, S. Tretiak, M.A. Alam, H.L. Wang, A.D. Mohite, Science, 347 (2015) 522-525.

[14] J.L. Burschka, N. Pellet, S.J. Moon, R. Humphry-Baker, P. Gao, M.K. Nazeeruddin, M. Grätzel, Nature, 499 (2013) 316-320.

[15] T. Leijtens, G.E. Eperon, S. Pathak, A. Abate, M.M. Lee, H.J. Snaith, Nature Communications, 4 (2013) 2885.

[16] Y.S. Liu, Z.R. Hong, Q. Chen, W.S. Chang, H.P. Zhou, T.B. Song, E. Young, Y. Yang, J.B. You, G. Li, Y. Yang, Nano Lett, 15 (2015) 662-668.

[17] W.J. Ke, G.J. Fang, J. Wang, P.L. Qin, H. Tao, H.W. Lei, Q. Liu, X. Dai, X.Z. Zhao, ACS Appl. Mater. Interfaces, 6 (2014) 15959-15965.

[18] Z.L. Ku, Y.G. Rong, M. Xu, T.F. Liu, H.W. Han, Scientific Reports, 3 (2013) 1-5.

[19] J.J. Shi, Y.H. Luo, H.Y. Wei, J.H. Luo, J. Dong, S.T. Lv, J.Y. Xiao, Y.Z. Xu, L.F. Zhu, X. Xu, H.J. Wu, D. M. Li, Q.B. Meng, ACS Appl. Mater. Interfaces, 6, (2014) 9711-9718.

[20] H.Y. Wang, Y. Wang, M. Yu, J. Han, Z.X. Guo, X.C. Ai, J.P. Zhang, Y.J. Qin, Phys. Chem. Chem. Phys, 18 (2016) 12128-12134.

[21] J.H. Heo, D.H. Song, H.J. Han, S.Y. Kim, J.H. Kim, D. Kim, H.W. Shin, T.K. Ahn, C. Wolf, T.W. Lee, S.H. Im, Adv Mater, 27 (2015) 3424-30.

[22] S.S. Chen, L. Lei, S.W. Yang, Y. Liu, Z.S. Wang, ACS Appl. Mater. Interfaces, 7 (2015) 25770-25776.

[23] Y.W. Li, Y. Zhao, Q. Chen, Y. Yang, Y.S. Liu, Z.R. Hong, Z.H. Liu, Y.T. Hsieh, L. Meng, Y.F. Li, Y. Yang, J. Am. Chem. Soc, 137 (2015) 15540-15547.

[24] T.H. Liu, K. Chen, Q. Hu, J. Wu, D.Y. Luo, S. Jia, R. Zhu, Q.H. Gong, Chinese Chemical Letters, 26 (2015) 1518-1521.

[25] K. Wang, C. Liu, P.C. Du, L. Chen, J.H. Zhu, A. Karim, X. Gong, Organic Electronics, 21 (2015) 19-26.

[26] F. Matteocci, Y. Busby, J.J. Pireaux, G. Divitini, S. Cacovich, C. Ducati, A.D. Carlo, ACS Appl. Mater. Interfaces, 7 (2015) 26176-26183.

[27] F.X. Xie, D. Zhang, H.M. Su, X.G. Ren, K.S. Wong, M. Grätzel, W. C. H. Choy, ACS Nano, 9 (2015) 639-646.

[28] D.Y. Liu, M.K. Gangishetty, T.L. Kelly, J. Mater. Chem. A, 2 (2014) 19873-19881.

[29] B. Zhang, M.J. Zhang, S.P. Pang, C.S. Huang, Z.M. Zhou, D. Wang, N. Wang, G.L. Cui, Adv. Mater. Interfaces, 3 (2016) 1600327.

[30] D.Y. Liu, T.L. Kelly, Nature Photonics, 8 (2014) 133-138.

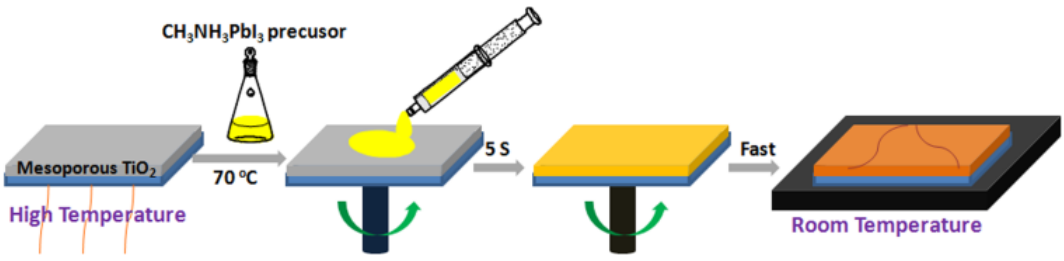

Scheme 1 Processing scheme for $CH_3NH_3PbI_3$-based thin-film on FTO/m-TiO_2 layer using hot-casting methods.

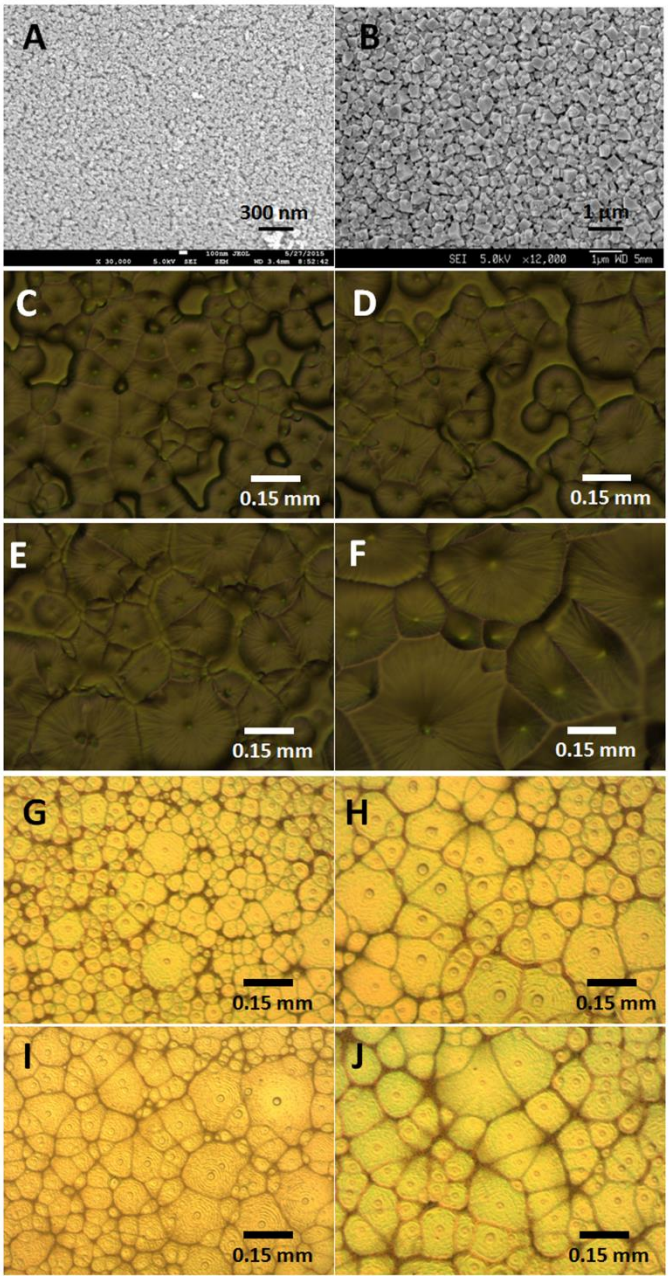

Fig. 1 SEM images of m-TiO_2 film prepared on FTO glass (A) and the $CH_3NH_3PbI_3$ film fabricated on FTO/m-TiO_2 by two-step method (B); Microscope images of $CH_3NH_3PbI_3$ films fabricated by hot-casting technique on FTO/m-TiO_2 substrates: using DMF solvent (100 mg/mL precusor solutions) separately at (C) 150 °C; (D) 160 °C; (E) 190 °C and (F) 175 °C; using GBL solution (100 mg/mL precusor solutions) separately at (G) 160 °C; (H) 170 °C; (I) 180 °C and (J) 190 °C.

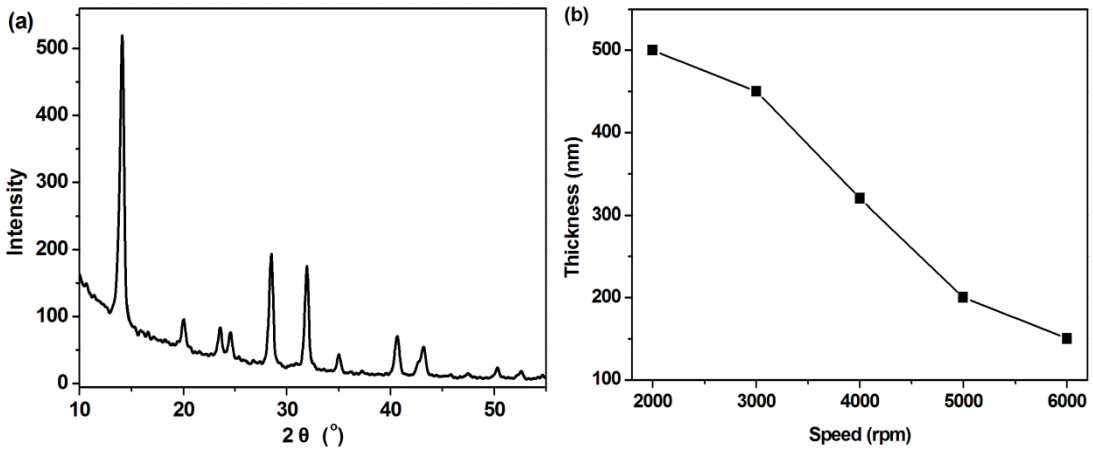

Fig. 2. (a) X-ray diffraction (XRD) profiles of $CH_3NH_3PbI_3$ films constructed on FTO/m-TiO_2 substrate by hot-casting technique using DMF solvent; (b) The thickness variation of $CH_3NH_3PbI_3$ films constructed on FTO/m-TiO_2 substrate with the speed variation of hot spin-coating using DMF as solvent for the precursor solution.

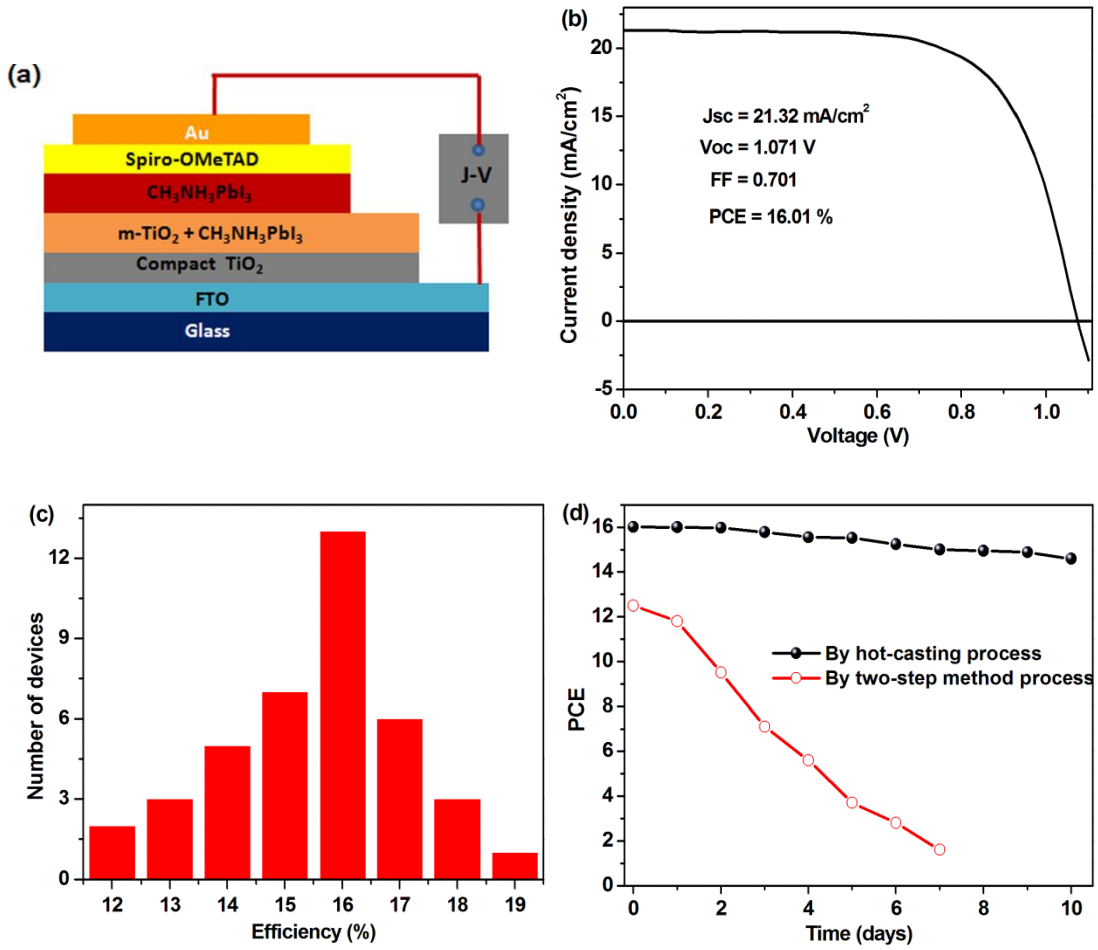

Fig. 3 (a) The device structure of $CH_3NH_3PbI_3$-based solar cells; (b) Current density-voltage curves of $CH_3NH_3PbI_3$-based devices fabricated on FTO/TiO_2 substrates by hot-casting technique using DMF as precursor solvent; (c) Histograms of device efficiency measured for 40 separate perovskite solar cells; (d) Stability of the $CH_3NH_3PbI_3$-based devices fabricated by hot-casting technique and two-step process.

Table 1 Photovoltaic parameters of the $CH_3NH_3PbI_3$-based device depending on the fabrication methods of $CH_3NH_3PbI_3$ film. These data were measured at AM 1.5G one sun illumination. Average values were obtained from 40 cells and relative humidity was about 50%.

$CH_3NH_3PbI_3$ film	Crystal size	Voc (V)	Jsc (mA/cm^2)	FF	PCE (%)
Hot-casting/DMF	200 nm	1.07 ± 0.013	21.32 ± 0.83	0.70 ± 0.01	16.01 ± 0.54
Hot-casting/GBL	0.20 mm	1.05 ± 0.009	20.70 ± 0.29	0.69 ± 0.01	14.80 ± 0.32
Two-step method	0.10 mm	1.05 ± 0.013	17.11 ± 0.70	0.68 ± 0.01	12.05 ± 0.46

GRAPHICAL ABSTRACT

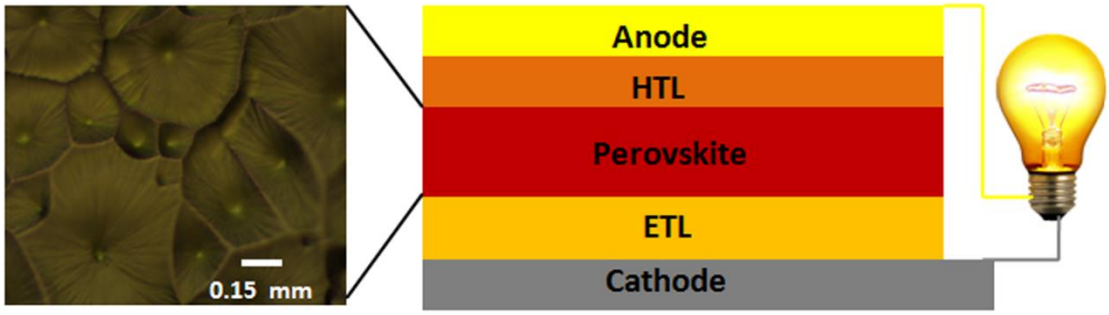

HIGHLIGHTS

- $CH_3NH_3PbI_3$ film with large crystal size of 0.5 mm was constructed on FTO/m-TiO_2 substrate by hot-casting technique.
- The PCE of the corresponding device fabricated by hot-casting method on FTO/m-TiO_2 (16.01%) was obviously better than the one by two-step method (12.50%).
- Excellent stability of the hot-casting-based device has been achieved, which remains at more than 91% under 55% humidity for 10 days.
- An important conclution can be confirmed that continuous and compact aggregation structure of $CH_3NH_3PbI_3$ films constructed by hot-casting technique was benefit for high performances perovskite solar cells.